PCCP

Spectral properties of a fluorescing molecule within a spherical metallic nanocavity†

Jörg Enderlein

Institute of Biological Information Processing 1, Forschungszentrum Jülich, D-52425 Jülich, Germany. E-mail: j.enderlein@fz-juelich.de

Received 15th January 2002, Accepted 14th February 2002
First published as an Advance Article on the web 7th May 2002

The electrodynamics of a fluorescing molecule (an electric dipole emitter) within a spherical metallic nanocavity is studied. It is shown that, for a favorable cavity size, the fluorescence properties such as fluorescence emission rate or photostability are strongly enhanced. This is caused by two effects: the enhancement of the exciting electromagnetic field within the cavity, and the dramatic reduction of the fluorescence lifetime due to the strong near-field interaction between dye and cavity. Both effects can largely outweigh the fluorescence losses caused by energy absorption within the cavity metal. Special emphasis is given to calculating the wavelength dependence of the fluorescence properties, allowing the modeling of real dyes with broad absorption and emission spectra. As an example of practical interest, the cavity-enhanced fluorescence properties of the widely used dye Rhodamine 6G are extensively studied. It is shown that the presence of the cavity also has a strong impact on the absorption and emission spectra of the dye. Last but not least, it is demonstrated that the interaction between dye and nanocavity can dramatically boost its fluorescence quantum yield.

Introduction

It is well known that the interaction of fluorescing molecules with metals can dramatically alter their fluorescence properties.[1–3] This is caused by three processes: (i) metal-mediated enhanced local intensity of the excitation light; (ii) energy transfer of the molecule's excited state energy to the metal; (iii) energy absorption within the metal. These three processes lead to several observable effects. The locally enhanced excitation intensity results in an enhanced optical excitation rate of the molecule, which can lead to a higher fluorescence emission rate. However, energy transfer to the metal together with absorption of the transferred energy therein counterbalances the enhanced excitation rate and may lead to complete quenching of any observable fluorescence. This is, for example, the case for molecules that are adsorbed directly on a metal surface. Furthermore, the energy transfer to the metal causes significant changes in the fluorescence lifetime of the molecule, by opening new channels for its return from the excited to the ground state. Under the assumption that photobleaching (irreversible photoinduced chemical destruction) can occur only as long as the molecule is in its excited state, a reduced excited lifetime leads to an increased photostability, in the sense of an increased average number of excitation cycles a molecule can undergo until photobleaching.[4] Thus, it may occur that, although the fluorescence emission rate is lowered by the presence of the metal, the average number of detectable fluorescence photons until photobleaching is increased. This can be important for single molecule detection experiments, where not only a high signal-to-background ratio is desirable (high fluorescence emission rate), but also a maximum number of detectable fluorescence photons until photobleaching. In ref. 5, these questions were addressed for molecules over planar metal/dielectric structures, and it was indeed found that for certain metals (silver, gold) and special geometries (metal film thickness, distance between fluorescing molecule and metal surface), the fluorescence properties can be as good as those for a similar situation without metal. In ref. 6, these studies were extended to a spherical metallic nanocavity, as shown in Fig. 1. Although one could expect that surrounding the fluorescing molecule with a closed metallic layer would lead to significant losses of fluorescence due to optical absorption within the metal, it was shown that for favorable cavity size and metal layer thickness, the fluorescence properties (emission rate and photostability) are dramatically enhanced. The study of ref. 6 was done for a single excitation and a single emission wavelength, not taking into account the broad absorption and emission spectra of real fluorescing molecules embedded in a solid or liquid environment at room temperature. In the present paper, an extended study of single molecule fluorescence within a spherical metallic nanocavity is presented, with special emphasis on the spectral dependence of the fluorescence excitation and emission properties. Knowledge of the spectral dependence allows us to calculate the fluorescence properties of real dyes within metallic nanocavities, as will be presented for the standard dye Rhodamine 6G. It will be shown that, in addition

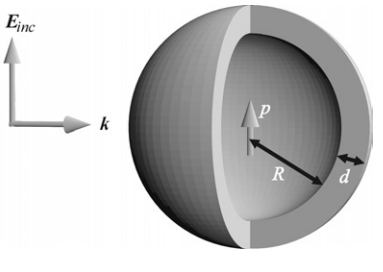

Fig. 1 Picture of the problem considered: A plane electromagnetic wave is incident onto a spherical dielectric bead with radius R coated with a thin metallic layer. At the bead's center, a dye molecule is positioned, with its excitation/emission dipole parallel to the electric field vector of the plane wave.

† Presented at the LANMAT 2001 Conference on the Interaction of Laser Radiation with Matter at Nanoscopic Scales: From Single Molecule Spectroscopy to Materials Processing, Venice, 3–6 October, 2001.

 DOI: 10.1039/b200502f

to the already mentioned changes in fluorescence emission rate, lifetime, and photostability, the absorption and emission spectra of a dye are also changed significantly, together with a dramatic increase in its fluorescence quantum yield.

Theory

The situation studied in this paper is depicted schematically in Fig. 1. A fluorescing molecule is positioned at the center of a metallic cavity, consisting of a homogenous dielectric bead with radius R and a thin metallic cover. The refractive indices of the bead material and the metal cover are denoted by η_b and η_m, respectively. The cavity is embedded within a homogeneous dielectric medium with refractive index η_w. The molecule is assumed to behave like an ideal electric dipole oscillator, with collinear absorption and emission dipole orientation. Fluorescence excitation is carried out by irradiating the cavity with a plane electromagnetic wave propagating perpendicular to the dipole orientation of the molecule, and it is assumed that this wave has an electric polarization parallel to the dipole orientation. By symmetry considerations one finds that at the center of the cavity the electric field is parallel to the dipole, even after interaction of the incident plane wave with the cavity. Thus, the excitation rate of an arbitrarily oriented molecule (or for arbitrarily oriented incident wave polarization) involves only an additional factor $\cos^2\Psi$, where Ψ is the angle between the dipole axis and the incident electric field polarization. In all subsequent calculations, the system without metal layer will be taken as reference, and all calculated quantities are always given with respect to their values for that reference system.

Excitation

The fluorescence excitation rate of the molecule is proportional to the square of the scalar product of the exciting electric field amplitude and the absorption dipole moment. Thus, one has to find the local electric field amplitude of the exciting field at the molecule's position (center of the cavity). Due to the spherical geometry of the studied system, it is advantageous to represent all fields as series expansions over vector spherical harmonics. In the present paper, the following notation for vector spherical harmonics will be used (in spherical coordinates r,θ,ϕ):

$$\boldsymbol{M}^f_{nm}(kr,\theta,\phi) = \sqrt{\frac{2n+1}{4\pi}\frac{(n-m)!}{(n+m)!}} \times \left[P^m_n \frac{\mathrm{i}m}{\sin\theta}\boldsymbol{e}_\theta - \left(P^{m+1}_n + m\cot\theta P^m_n\right)\boldsymbol{e}_\phi\right] f_n \mathrm{e}^{\mathrm{i}m\phi}, \tag{1a}$$

$$\boldsymbol{N}^f_{nm}(kr,\theta,\phi) = \sqrt{\frac{2n+1}{4\pi}\frac{(n-m)!}{(n+m)!}} \times \left\{\frac{n(n+1)}{kr} f_n P^m_n \mathrm{e}^{\mathrm{i}m\phi}\boldsymbol{e}_r + \frac{1}{2}\left(\frac{f_n}{kr} + f_{n-1} - f_{n+1}\right) \times \left[\left(P^{m+1}_n + m\cot\theta P^m_n\right)\boldsymbol{e}_\theta + \frac{\mathrm{i}m}{\sin\theta} P^m_n \boldsymbol{e}_\phi\right]\mathrm{e}^{\mathrm{i}m\phi}\right\}. \tag{1b}$$

Here, n and $m \leqslant n$ are non-negative integer numbers enumerating the harmonics, $P_n{}^m$ are associated Legendre polynomials[7] of the variable $\cos\theta$, f_n denote spherical Bessel functions[7] with argument kr, where k is the wave vector of the electromagnetic field, and the $\boldsymbol{e}_{r,\theta,\phi}$ are unit vectors. These vector spherical harmonics constitute a complete set of orthogonal functions that fulfill the vector wave equation, namely $\Delta\boldsymbol{M} + k^2\boldsymbol{M} = 0$, together with the zero-divergence condition div $\boldsymbol{M} = 0$ (similarly for $\boldsymbol{N}$). Additionally, the harmonics are connected by the relations rot $\boldsymbol{M} = k\boldsymbol{N}$ and rot $\boldsymbol{N} = k\boldsymbol{M}$. The harmonics for negative values of m, $|m| \leqslant n$, are given by the complex conjugate expressions of $\boldsymbol{M}_{n|m|}{}^f$ and $\boldsymbol{N}_{n|m|}{}^f$, respectively.

If the incident plane wave propagates along the z-direction ($\theta = 0$) and has a polarization along the x-direction ($\theta = \pi/2$ and $\phi = 0$), its electric and magnetic field amplitudes are given by[8]

$$\boldsymbol{E}_0 = \sum_{n=1}^{\infty} i^{n+1}\sqrt{\frac{4\pi(2n+1)}{n(n+1)}}(\boldsymbol{N}^j_{n,1} + \boldsymbol{M}^j_{n,1} + \boldsymbol{N}^j_{n,-1} - \boldsymbol{M}^j_{n,-1}) \tag{2}$$

and

$$\boldsymbol{B}_0 = -\mathrm{i}k_0^{-1}\mathrm{rot}\,\boldsymbol{E} = \eta_w \sum_{n=1}^{\infty} \mathrm{i}^n\sqrt{\frac{4\pi(2n+1)}{n(n+1)}}(\boldsymbol{N}^j_{n,1} + \boldsymbol{M}^j_{n,1} - \boldsymbol{N}^j_{n,-1} + \boldsymbol{M}^j_{n,-1}), \tag{3}$$

where an $\mathrm{e}^{-\mathrm{i}\omega t}$-temporal dependence of all fields was assumed, with ω being the oscillation frequency of the excitation light. The superscript j stands for the modified Bessel functions of the first kind, and the radial coordinate argument in all functions is $k_w r$, with $k_w = \eta_w k_0$ and k_0 being the wave vector lengths of the excitation light in the cavity's surrounding medium and in vacuum, respectively.

To obtain the electric field after interaction of the plane wave with the cavity, one adopts representations similar to eqn. (2) for the electric and magnetic fields within the cavity's core ($\boldsymbol{E}_b$, $\boldsymbol{B}_b$) and shell ($\boldsymbol{E}_m$, $\boldsymbol{B}_m$), and for the scattered field outside the cavity ($\boldsymbol{E}_s$, $\boldsymbol{B}_s$), however with unknown coefficients a and b, namely

$$\boldsymbol{E}_s = \sum_{n=1}^{\infty}[a_n^{(s)}(\boldsymbol{M}^h_{n,1} - \boldsymbol{M}^h_{n,-1}) + b_n^{(s)}(\boldsymbol{N}^h_{n,1} + \boldsymbol{N}^h_{n,-1})], \tag{4a}$$

$$\boldsymbol{E}_m = \sum_{n=1}^{\infty}\Big[a_n^{(m,j)}(\boldsymbol{M}^j_{n,1} - \boldsymbol{M}^j_{n,-1}) + b_n^{(m,j)}(\boldsymbol{N}^j_{n,1} + \boldsymbol{N}^j_{n,-1}) + a_n^{(m,h)}(\boldsymbol{M}^h_{n,1} - \boldsymbol{M}^h_{n,-1}) + b_n^{(m,h)}(\boldsymbol{N}^h_{n,1} + \boldsymbol{N}^h_{n,-1})\Big], \tag{4b}$$

$$\boldsymbol{E}_b = \sum_{n=1}^{\infty}[a_n^{(b)}(\boldsymbol{M}^j_{n,1} - \boldsymbol{M}^j_{n,-1}) + b_n^{(b)}(\boldsymbol{N}^j_{n,1} + \boldsymbol{N}^j_{n,-1})]. \tag{4c}$$

Here, the superscript h denotes spherical Bessel functions of the third kind (spherical Hankel functions), so that $\boldsymbol{E}_s$ obeys Sommerfeld's radiation condition for outgoing waves. The radial coordinate arguments in the functions involved are $k_w r$, $k_m r$ and $k_b r$ for the $\boldsymbol{E}_s$, $\boldsymbol{E}_m$, $\boldsymbol{E}_b$, respectively, where the $k_{w,m,b}$ are, as before, the wave vector lengths in the different media. The magnetic field amplitudes are found by applying the operator $-\mathrm{i}k_0^{-1}$rot to the above electric field amplitudes.

The electric and magnetic field amplitudes in the different regions have to fulfill the boundary conditions for electromagnetic fields at the inner and outer boundary of the metal layer, namely, that the tangential components of the electric and magnetic fields have to be equal on both sides of a boundary. For every order n of the above expansions, this yields a total of eight linear algebraic equations for the eight unknown coefficients, which can be solved in a straightforward way.

The situation dramatically simplifies if one is interested only in the electric field value at the cavity's center, because for $r = 0$ the only non-vanishing expressions involving Bessel functions are $j_0(0) = 1$ and $\lim_{x\to 0} j_1(x)/x = 1/3$. Taking into

account also that $\lim_{\theta\to 0} P_1^1(\cos\theta)/\sin\theta = 1$ and $P_1^2(1) = 0$, one finds the simple expression

$$|\boldsymbol{E}_\mathrm{b}(0,0,0)|^2 = \frac{\left|b_1^{(b)}\right|^2}{6\pi}. \tag{5}$$

Thus, to obtain the fluorescence excitation rate at the cavity's center one has to solve the boundary condition equations only at order $n = 1$.

Emission

The interaction of the radiating molecule with the cavity can be found similarly to the excitation field amplitude in the preceding subsection. The electric field amplitude of a freely oscillating dipole with orientation along the z-direction ($\theta = 0$) placed within a homogenous dielectric medium with refractive index η_b is given by[9]

$$\begin{aligned}\boldsymbol{E}_\mathrm{D} &= \frac{\mathrm{i}k_0^2 p}{k_\mathrm{b} r}\left\{ -\frac{2}{k_\mathrm{b} r}\left(1+\frac{\mathrm{i}}{k_\mathrm{b} r}\right)\cos\theta\,\boldsymbol{e}_r \right. \\ &\qquad \left. + \left(\mathrm{i} - \frac{1}{k_b r} - \frac{\mathrm{i}}{(k_b r)^2}\right)\sin\theta \boldsymbol{e}_\theta \right\} \mathrm{e}^{\mathrm{i}k_b r} \\ &= \mathrm{i}\sqrt{\frac{4\pi}{3}} p \eta_\mathrm{b} k_0^3 \boldsymbol{N}_{1,0}^h, \end{aligned} \tag{6}$$

where p is the amplitude of the oscillating dipole. Analogous to the preceding subsection, the field amplitudes within the different media are represented by expressions similar to that of the free dipole field, namely

$$\boldsymbol{E}_\mathrm{s} = c^{(s)} \boldsymbol{N}_{1,0}^h, \tag{7a}$$

$$\boldsymbol{E}_\mathrm{m} = c^{(m,1)} \boldsymbol{N}_{1,0}^j + c^{(m,2)} \boldsymbol{N}_{1,0}^h, \tag{7b}$$

$$\boldsymbol{E}_\mathrm{b} = c^{(b)} \boldsymbol{N}_{1,0}^j. \tag{7c}$$

Here, $\boldsymbol{E}_\mathrm{b}$ is the reaction field inside the cavity, arising from the interaction of the dipole with the cavity. The four unknown coefficients in the above equations are again found as solutions of the boundary conditions.

Two quantities are of major interest when considering the molecule's fluorescence emission: the lifetime of its excited state, and the energy transmission through the metal layer (*i.e.* the probability that the dipole's energy is emitted away from the cavity). To obtain both values, one calculates the energy fluxes S_in and S_out through the inner and outer surface of the metallic layer. If there are no non-radiative transition channels from the excited to the ground state (unity fluorescence quantum yield), then the excited state lifetime is proportional to $1/S_\mathrm{in}$. Moreover, the probability that the dipole's energy is radiated away from the cavity and is not absorbed within the metal layer is given by $S_\mathrm{out}/S_\mathrm{in}$.

Knowing the electric and magnetic field amplitudes allows calculation of S_in and S_out by integrating the Poynting vector over the corresponding surfaces, *i.e.*

$$\begin{aligned} S_\mathrm{in} &= \mathrm{Re}\left[\int_{r=R} (\boldsymbol{E}_\mathrm{in} \times \boldsymbol{B}_\mathrm{in})\mathrm{d}\boldsymbol{A}\right] \\ &= \frac{1}{k_0}\mathrm{Re}\left[\mathrm{i}\int_{r=R} (\boldsymbol{E}_\mathrm{in} \times \mathrm{rot}\,\boldsymbol{E}_\mathrm{in})\mathrm{d}\boldsymbol{A}\right] \\ &= \frac{8\pi}{3}\eta_\mathrm{b} k_0^4 p^2 + 4\sqrt{\frac{\pi}{3}} k_0 p\,\mathrm{Im}[c^{(b)}] \end{aligned} \tag{8}$$

where $\boldsymbol{E}_\mathrm{in} = \boldsymbol{E}_\mathrm{D} + \boldsymbol{E}_\mathrm{b}$. Analogously, one finds

$$S_\mathrm{out} = \mathrm{Re}\left[\int_{r=R+d} (\boldsymbol{E}_\mathrm{w} \times \boldsymbol{B}_\mathrm{w})\mathrm{d}\boldsymbol{A}\right] = \frac{2}{\eta_\mathrm{w} k_0^2}\left|c^{(w)}\right|^2, \tag{9}$$

where the integration is now done over the exterior surface of the cavity. In calculating the above energy fluxes, a constant factor equal to the vacuum speed of light divided by 8π was omitted.

Numerical results

General results

For the subsequent numerical studies, the following material constants were used. The cavity core is assumed to be a polymeric or glassy dielectric with a refractive index of $\eta_\mathrm{b} = 1.5$, close to the value of glass. The metal is assumed to be silver, and for its wavelength dependent refractive index η_m bulk values were used, employing a Brendel–Bormann model.[10] This is, of course, an approximation neglecting any effects such as spatial electron confinement or non-locality of the dielectric constant (for a comprehensive discussion see ref. 11 and references therein). The surrounding medium was assumed to be water with a refractive index of $\eta_\mathrm{w} = 1.33$. Both η_b and η_w are assumed to be constant over the whole range of considered wavelengths (300–800 nm), thus neglecting the optical dispersion of the bead material and the surrounding medium, which is in both cases much weaker than that of silver. For simplicity it is assumed that the molecule has unity fluorescence quantum yield; the more general case will be considered at the end of this section.

The first question of interest is how much the fluorescence excitation rate I_ex is enhanced by the presence of the metal layer. The excitation rate is directly proportional to the absolute square value of the electric field amplitude at the cavity's center, which is calculated as described in the preceding section. Excitation enhancement by the presence of the metal is thus given by

$$\frac{I_\mathrm{ex}}{I_\mathrm{ex,0}} = \frac{|\boldsymbol{E}_\mathrm{b}(0,0,0)|^2}{\left|\boldsymbol{E}_\mathrm{b,0}(0,0,0)\right|^2} \tag{10}$$

where the subscript zero refers always to the reference system of a bead without metal cover. Calculations were performed for both the bead without metal cover, and a cavity with a metal cover of 5 nm thickness. The choice of this value is the result of the study in ref. 6, which shows that optimal fluorescence properties for cavity-enclosed dyes are achieved at very small values of metal layer thickness. However, it is not reasonable to perform calculations for thickness values much below 5 nm, due to the breakdown of classical continuum electrodynamics at very small length scales.[12,13] When calculating excitation rate enhancements, excitation wavelengths between 300 nm and 800 nm were considered, and the cavity's inner radius was varied between 5 nm and 45 nm. In Fig. 2, the enhancement of the excitation rate is shown relative to the reference system of the bead without metal cover. For a narrow range of excitation wavelengths and bead radii, enhancement factors of up to 300 are achieved. However, this value alone does not give any information about detectable fluorescence brightness if it is not known how much of the energy of the molecule's excited state is transmitted through the metal layer. As mentioned above, for a molecule with unity fluorescence quantum yield, the probability that the excited state energy is radiated away and not absorbed by the metal is given by the ratio $S_\mathrm{out}/S_\mathrm{in}$ (without metal layer, the ratio $S_\mathrm{out}/S_\mathrm{in}$ is always unity). The numerical result is shown in Fig. 3, where emission wavelengths between 400 nm and 800 nm have been considered. For a certain bead radius, excitation wavelength, and emission wavelength, the enhancement of the fluorescence emission rate is the product of the corresponding excitation enhancement (Fig. 2) and the transmission factor $S_\mathrm{out}/S_\mathrm{in}$ (Fig. 3).

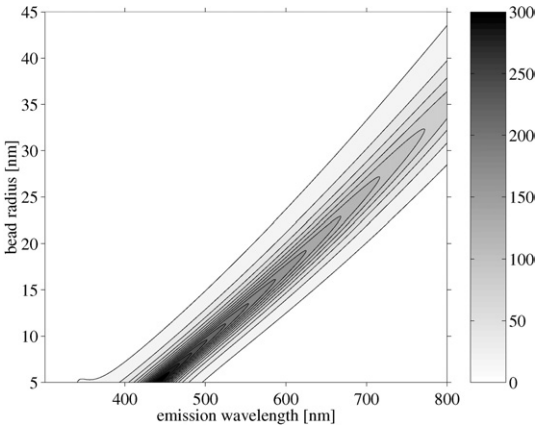

Fig. 2 Dependence of the excitation intensity enhancement $I_{ex}/I_{ex,0}$ on bead radius R and excitation wavelength λ.

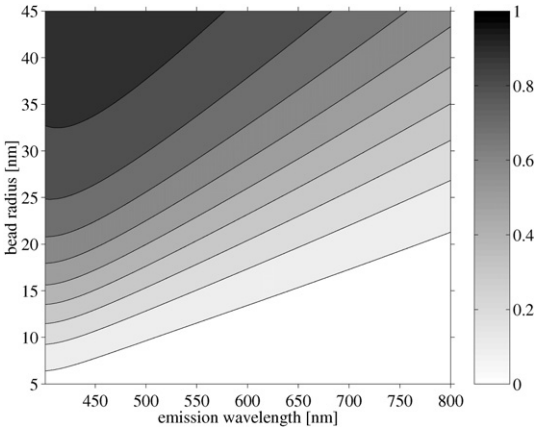

Fig. 3 Dependence of the transmission factor S_{out}/S_{in} on bead radius R and emission wavelength λ.

The next quantity of interest is the change in the excited state lifetime. For a molecule with unity fluorescence quantum yield, this lifetime is inversely proportional to the energy flux S_{in}, or

$$\frac{\tau}{\tau_0} = \frac{S_0}{S_{in}}, \tag{11}$$

where S_0 is the energy flux for the uncovered bead, and τ_0 the fluorescence lifetime of the dye embedded in an uncovered bead. The lifetime reduction τ/τ_0 is shown in Fig. 4, displaying lifetime changes of more than three orders of magnitude, at nearly the same wavelength and bead radius values as those where maximum excitation enhancement is achieved. However, real fluorophores always show a non-vanishing Stokes shift between maximum absorption and emission wavelengths, so that maximum lifetime reduction occurs at a different cavity size than maximum excitation enhancement. If one assumes that photobleaching of a molecule can happen only while it is in the excited state, a reduced excited state lifetime leads directly to an enhanced photostability. However, the number of interest is not the average number of excitation cycles a molecule undergoes until photobleaching, but the average number N of emitted fluorescence photons. This number is inversely proportional to the excited state lifetime multiplied by the transmission factor S_{out}/S_{in}, *i.e.* it is directly proportional to S_{out},

$$\frac{N}{N_0} = \frac{S_{out}}{S_0}. \tag{12}$$

Curiously, for the special case of a molecule placed at the cavity's center, the increase in N/N_0 equals exactly the increase in

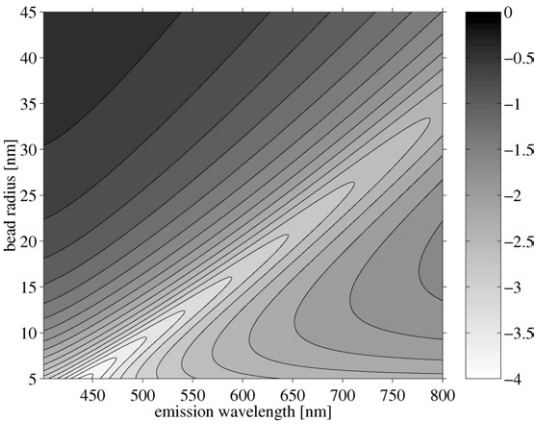

Fig. 4 Dependence of the decadic logarithm lifetime reduction, $\log \tau/\tau_0$, on bead radius R and emission wavelength λ.

excitation intensity as presented in Fig. 2. This can be seen when taking into account that the excitation intensity at the cavity's center is proportional to the absolute square of b_1, *cf.* eqn. (5), whereas S_{out} is proportional to the absolute square of $c^{(w)}$, *cf.* eqn. (9). However, the functional term corresponding to b_1 in the expansions of eqns. (2) and (4) has the explicit form:

$$\begin{aligned} \boldsymbol{N}^j_{1,1} + \boldsymbol{N}^j_{1,-1} = \sqrt{\frac{3}{2\pi}} \Bigg\{ & -\frac{2}{kr}\left(\frac{\sin kr}{(kr)^2} - \frac{\cos kr}{kr}\right) \sin\theta\cos\phi\, \boldsymbol{e}_r \\ & + \left(-\frac{\sin kr}{(kr)^3} + \frac{\cos kr}{(kr)^2} + \frac{\sin kr}{kr}\right) \\ & \times [-\cos\theta\cos\phi\, \boldsymbol{e}_\theta + \sin\phi\, \boldsymbol{e}_\phi] \Bigg\}. \end{aligned} \tag{13}$$

which is nothing else than the real part of the electric field amplitude of an oscillating dipole with orientation along the x-axis ($\theta = \pi/2, \phi = 0$). Thus, solving for the b_1 of the plane wave/cavity interaction is mathematically similar to solving for $c^{(w)}$ of the dipole/cavity interaction, leading indeed to identical enhancement factors for the excitation and for the average number of emitted fluorescence photons until photobleaching. Thus, Fig. 2 shows that the number of extractable fluorescence photons until photobleaching can be up to 300 times larger for a dye in the metal cavity than the number for a dye in a bead without cover.

Case study: Rhodamine 6G

All considerations of the preceding subsection refer to a dye with perfectly monochromatic excitation and emission. However, real dyes at room temperature show broad excitation and emission spectra. Fortunately, the derived results for the wavelength dependence of excitation enhancement, transmission factor S_{out}/S_{in}, and fluorescence lifetime also allow us to predict the fluorescence properties of such molecules. Consider a dye with wavelength dependent absorption cross section $\sigma_0(\lambda)$ and emission spectrum $F_0(\lambda)$. Due to the wavelength dependence of the excitation enhancement, the apparent absorption spectrum $\sigma(R,\lambda)$ of the dye in the cavity will be proportional to the product of $\sigma_0(\lambda)$ and the excitation enhancement at wavelength λ, *i.e.*

$$\frac{\sigma(R,\lambda)}{\sigma_0(\lambda)} = \frac{I_{ex}(R,\lambda)}{I_{ex,0}(R)}. \tag{14}$$

As an example of practical concern, computations were made for the widely used dye Rhodamine 6G. Its bulk absorption and emission spectra were taken from ref. 14. For the sake

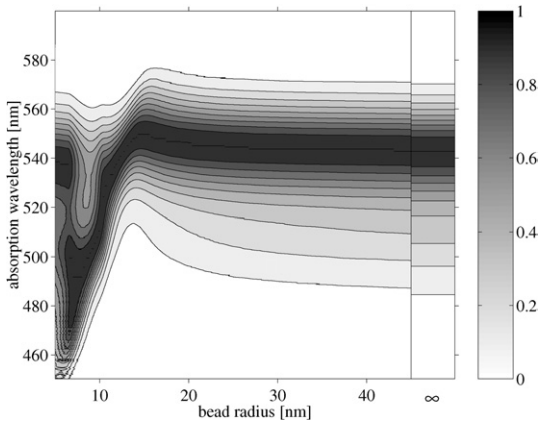

Fig. 5 Dependence of the absorption spectrum of Rhodamine 6G on bead radius R. For comparison, the bulk spectrum is also shown ($R = \infty$).

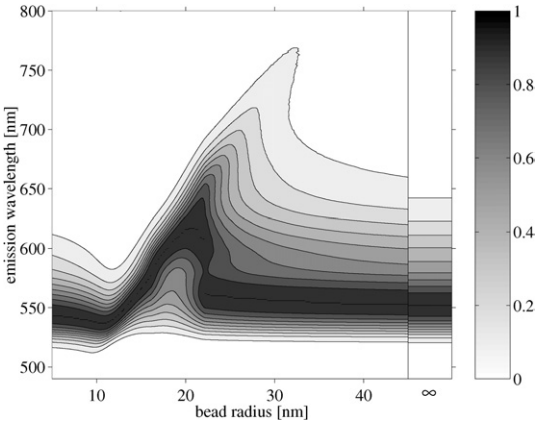

Fig. 6 Dependence of the emission spectrum of Rhodamine 6G on bead radius R. For comparison, the bulk spectrum is also shown ($R = \infty$).

of simplicity, the subsequent calculations adopt the value one for the fluorescence quantum yield. Fig. 5 shows the apparent absorption spectrum of a Rhodamine 6G molecule in a cavity for different values of inner radius. As can be seen, the absorption maximum shifts considerably in wavelength space, as well as the width of the spectrum.

Calculating the altered emission spectrum is more involving. One has to recall that the transition rate $k_0(\lambda)$ from the excited state to the ground state at a given wavelength λ is proportional to the value of the normalized emission spectrum $F_0(\lambda)$ at this wavelength divided by the excited state lifetime τ_0, $k_0(\lambda) = F_0(\lambda)/\tau_0$. Or, *vice versa*, the excited state lifetime is given by the inverse of the integral of these transition rates, integrated over all wavelengths.

$$\frac{1}{\tau_0} = \int \mathrm{d}\lambda k_0(\lambda). \tag{15}$$

The presence of the cavity changes the transition rates in a wavelength dependent manner, as displayed by Fig. 4. The observable emission spectrum $F(R,\lambda)$ of a cavity-enclosed dye is proportional to these changed transition rates times the transmission factor $S_{\mathrm{out}}/S_{\mathrm{in}}$, *i.e.*

$$\begin{aligned} F(R,\lambda) &\propto \frac{F_0(\lambda)}{\tau_0(R)} \frac{\tau_0(R)}{\tau(R,\lambda)} \frac{S_{\mathrm{out}}(R,\lambda)}{S_{\mathrm{in}}(R,\lambda)} \\ &= F_0(\lambda) \frac{S_{\mathrm{out}}(R,\lambda)}{S_0(R)}, \end{aligned} \tag{16}$$

where $\tau_0(R)$ is the excited state lifetime of the dye in the bead without metal cover, and $\tau_0(R)/\tau(R,\lambda)$ is the cavity induced enhancement of the transition rate at wavelength λ. For a Rhodamine 6G dye, the resulting emission spectra at different bead radii are displayed in Fig. 6.

On the basis of the excitation and emission spectra at different cavity sizes the enhancement of overall fluorescence brightness I_{em} can be calculated. Fluorescence brightness is understood as the observable fluorescence emission rate, and it is given by the excitation rate at the excitation wavelength times the integral over the product of transition rate F_0/τ and transmission factor $S_{\mathrm{out}}/S_{\mathrm{in}}$, *i.e.*

$$\begin{aligned} \frac{I_{\mathrm{em}}(R,\lambda_{\mathrm{ex}})}{I_{\mathrm{em},0}(R)} &= \frac{I_{\mathrm{ex}}(R,\lambda_{\mathrm{ex}})}{I_{\mathrm{ex},0}(R)} \left(\int \mathrm{d}\lambda \frac{F_0(\lambda)}{\tau(R,\lambda)} \frac{S_{\mathrm{out}}(R,\lambda)}{S_{\mathrm{in}}(R,\lambda)} \right) \Bigg/ \\ \left(\int \mathrm{d}\lambda \frac{F_0(\lambda)}{\tau_0(R)} \right) &= \frac{I_{\mathrm{ex}}(R,\lambda_{\mathrm{ex}})}{I_{\mathrm{ex},0}(R)} \int \mathrm{d}\lambda F_0(\lambda) \frac{S_{\mathrm{out}}(R,\lambda)}{S_0(R)}. \end{aligned} \tag{17}$$

In the last line, it was taken into account that $F_0(\lambda)$ is assumed to be normalized, $\int \mathrm{d}\lambda F_0(\lambda) = 1$. The enhancement of the fluorescence brightness at three typical excitation laser wavelengths

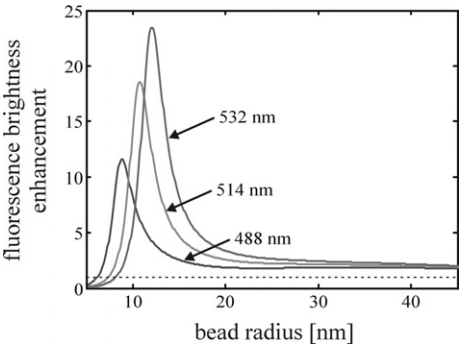

Fig. 7 Fluorescence brightness enhancement of Rhodamine 6G at three different excitation wavelengths.

is shown in Fig. 7. Maximum fluorescence brightness occurs at 532 nm excitation wavelength, as one would expect by inspecting the absorption spectrum, with an enhancement close to a remarkable factor of 25 for a bead radius of *ca.* 12 nm.

The apparent reduction in excited state lifetime, *i.e.* the fluorescence lifetime value that one would measure in a fluorescence lifetime measurement, can be derived when taking into account that eqn. (15) is a general relation valid also for a cavity-enclosed dye. Thus, the measurable lifetime is given by the integral

$$\frac{1}{\bar{\tau}(R)} = \int \mathrm{d}\lambda \frac{F_0(\lambda)}{\tau(R,\lambda)}. \tag{18}$$

The lifetime reduction $\bar{\tau}(R)/\tau_0(R)$ for a Rhodamine 6G molecule is depicted in Fig. 8. The lifetime reduction leads to an enhancement of the overall photostability of the dye, or more precisely, how many fluorescence photons it emits until photobleaching. Analogous to the explanation in the preceding subsection, this number equals the weighted integral of $\tau_0 S_{\mathrm{out}}/\tau S_{\mathrm{in}}$, using the emission spectrum as weight function, *i.e.*

$$\begin{aligned} \frac{N(R)}{N_0(R)} &= \int \mathrm{d}\lambda F_0(\lambda) \frac{\tau_0(R)}{\tau(R,\lambda)} \frac{S_{\mathrm{out}}(R,\lambda)}{S_{\mathrm{in}}(R,\lambda)} \Bigg/ \int \mathrm{d}\lambda F_0(\lambda) \\ &= \int \mathrm{d}\lambda F_0(\lambda) \frac{S_{\mathrm{out}}(R,\lambda)}{S_0(R)}. \end{aligned} \tag{19}$$

The bead radius dependence of the enhancement N/N_0 for Rhodamine 6G is shown in Fig. 9. To illustrate once more the spectral changes of the emission spectrum, Fig. 10 compares the emission spectra of a Rhodamine 6G dye in bulk and in a cavity with a size that yields maximum photostability, *i.e.* a size most desirable in practical applications. Considerable

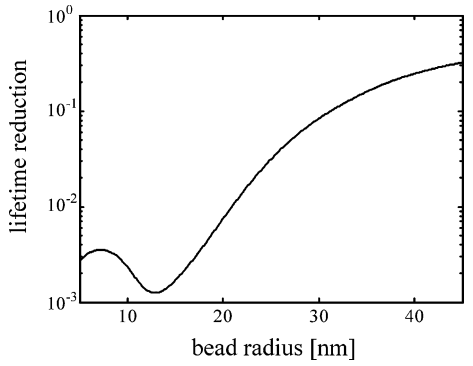

Fig. 8 Fluorescence lifetime reduction $\bar{\tau}/\tau_0$ for Rhodamine 6G.

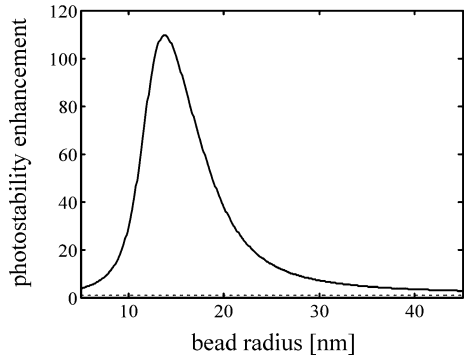

Fig. 9 Increase in number of detectable fluorescence photons N/N_0 for Rhodamine 6G.

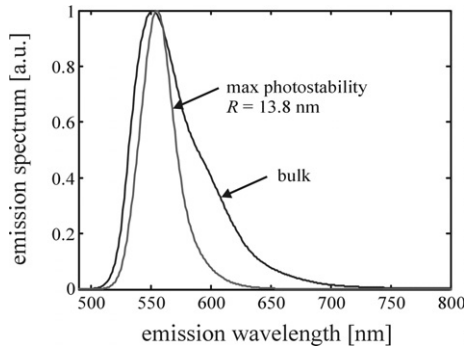

Fig. 10 Comparison between the emission spectrum of Rhodamine 6G in a cavity with size yielding maximum photostability, and the bulk spectrum of Rhodamine 6G.

narrowing of the emission spectrum can be seen, due to the resonance character of the lifetime reduction in dependence on emission wavelength (Fig. 4).

Last but not least, let us consider what happens if the bare dye's fluorescence quantum yield Φ_0 is not unity. The fluorescence quantum yield is defined as the ratio of the radiative decay rate $k_{r,0}$ of the excited state (leading to the emission of a fluorescence photon) to the complete decay rate $k_{r,0}+k_{nr}$ (measurable through the fluorescence lifetime), including also non-radiative de-excitation processes (k_{nr}), *i.e.*

$$\Phi_0 = \frac{k_{r,0}}{k_{r,0}+k_{nr}}. \tag{20}$$

The presence of the metal cavity significantly changes the overall radiative transition rate according to the relation

$$\frac{k_r}{k_{r,0}} = \frac{\tau_0}{\bar{\tau}}. \tag{21}$$

If the presence of the cavity does not change the non-radiative

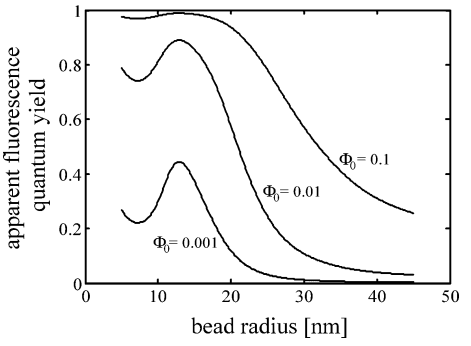

Fig. 11 Enhancement of the fluorescence quantum yield Φ of a hypothetical dye with the same spectral properties as Rhodamine 6G but with different values of Φ_0.

decay processes, the fluorescence quantum yield of the cavity-enclosed dye is given by

$$\Phi = \frac{k_r}{k_r+k_{nr}} = \frac{\Phi_0}{\Phi_0+(1-\Phi_0)\bar{\tau}(R)/\tau_0(R)}. \tag{22}$$

In Fig. 11, the fluorescence quantum yields in dependence on the bead radius are shown for three different initial values of Φ_0. It should be emphasized that in the expression for Φ no absorption losses within the metal layer are taken into account. Thus, a value of Φ close to one does not mean that every excitation cycle of the molecule generates a detectable fluorescence photon. However, the value of Φ is a direct measure of how important non-radiative decay processes are. As can be seen in Fig. 11, the increase in Φ can be tremendous, converting a barely fluorescing dye into an excellent emitter.

Conclusion

It was shown that the enclosure of a fluorescing dye in a metallic nanocavity can lead, for a favorable cavity size, to tremendous enhancements of its fluorescence properties such as brightness (fluorescence emission rate), photostability (number of detectable fluorescence photons until photobleaching), and quantum yield. Also, its lifetime is reduced by orders of magnitude. The latter can be important, besides leading to an enhanced photostability, if one is interested in converting fluorescence dyes with long decay times (*e.g.* europium dyes with fluorescence decay times in the microsecond range) into dyes with short decay time, thus significantly increasing their optical saturation intensity.

In the present paper, all calculations were performed for a spherical cavity, and for a single fluorophore at the cavity's center. Future work will study fluorescing molecules at arbitrary locations within the cavity, as well as in cavities with non-spherical shape.

Acknowledgement

Financial support by the Volkswagenstiftung (Grant I/76064) is gratefully acknowledged. I thank Martin Böhmer for many inspiring discussions. I thank Eike Stedefeldt for his enduring and exceedingly helpful support of my work.

References

1 E. M. Purcell, *Phys. Rev.*, 1947, **69**, 681.
2 K. H. Drexhage, *Progr. Opt.*, 1974, **XII**, 165–232.
3 R. R. Chance, A. Prock and R. Silbey, *Adv. Chem. Phys.*, 1978, **37**, 1–65.

4 J. Enderlein, *Chem. Phys.*, 1999, **247**, 1–9.
5 J. Enderlein, *Biophys. J.*, 2000, **78**, 2151–8.
6 J. Enderlein, *Appl. Phys. Lett.*, 2002, **80**, 315–7.
7 *Handbook of Mathematical Functions*, ed. M. Abramowitz and I. A. Stegun, Harry Deutsch, Thun/Frankfurt a.M., 1984.
8 H. C. van de Hulst, *Light Scattering by Small Particles*, Dover, London, 1981.
9 J. D. Jackson, *Classical Electrodynamics*, Wiley, New York, 1975, p. 278.
10 A. D. Rakic, A. B. Djurišic, J. M. Elazar and M. L. Majewski, *Appl. Opt.*, 1998, **37**, 5271–83.
11 M. Moskovits, *Rev. Mod. Phys.*, 1985, **57**, 783–826.
12 C. Girard, A. Dereux and O. J. F. Martin, *Phys. Rev. B*, 1994, **49**, 13872–81.
13 F. J. Garcia-Vidal and J. B. Pendry, *Phys. Rev. Lett.*, 1996, **77**, 1163–6.
14 H. Du, R. A. Fuh, J. Li, A. Corkan and J. S. Lindsey, *Photochem. Photobiol.*, 1998, **68**, 141–2.